PHYSICAL REVIEW B **88**, 121401(R) (2013)

Interference of topologically protected edge states in silicene nanoribbons

Motohiko Ezawa[1] and Naoto Nagaosa[1,2]
[1]*Department of Applied Physics, University of Tokyo, Hongo 7-3-1, 113-8656, Japan*
[2]*RIKEN Center for Emergent Matter Science (CEMS), Wako 351-0198, Japan*
(Received 28 January 2013; published 3 September 2013)

Silicene is a graphene-like honeycomb structure made of silicon atoms. It is a two-dimensional quantum spin-Hall insulator due to the spin-orbit interaction. According to the bulk-edge correspondence we expect zero-energy edge channels to appear in silicene nanoribbons. The behaviors of the helical edge channels are completely different between the armchair and the zigzag edges. Zero-energy states disappear in armchair nanoribbons despite the bulk-edge correspondence, while they appear as zigzag nanoribbons even if the width is quite narrow. The difference originates in the penetration depth of the helical edge channel, which is antiproportional to the spin-orbit gap for the armchair edge, while it remains as short as the lattice constant for the zigzag edge. These properties make clear distinctions between silicene and graphene nanoribbons, especially for armchair edges: In silicene edge states emerge as required by its topology, though the zero-energy states disappear from the energy spectrum, whereas in graphene no edge states exist. The emergence of edge states in armchair nanoribbons must be experimentally detectable by scanning tunneling microscopy, and may well serve as an experimental signal that silicene is a topological insulator.

DOI: 10.1103/PhysRevB.88.121401 PACS number(s): 73.63.−b, 73.20.At, 75.70.Tj, 81.05.ue

Silicene, a monolayer honeycomb structure of silicon atoms, is attracting intensive interest due to its experimental realization[1–5] in 2012. It is a graphene analog of silicon, which similarly has Dirac cones at the K and K' points in the Brillouin zone. Silicene has a richer physics than graphene due to its relatively large spin-orbit interaction (SOI), which naturally realizes quantum spin-Hall (QSH) effects[6] originally proposed[7] but unrealistic[8,9] in graphene. Silicene has another advantage; that is, the gap is tunable in various external ways such as by applying electric field,[10] photoirradiation,[11] and antiferromagnetic exchange interactions.[12] Silicene has enormously rich physics[10–13] in view of topological insulators.

Topological insulator is a new state of matter characterized by topological numbers.[14,15] A powerful tool to determine whether the system is topological is to employ the bulk-edge correspondence.[14,15] The system is topological when there are zero-energy edge states,[16–18] while it is trivial when there are not.

There are two types of edges, i.e., the zigzag edge and the armchair edge [Figs. 1(a) and 1(b)]. Let us review the edge channels of graphene nanoribbons.[19–21] The zigzag edge is characterized by strictly localized edge channels at the outermost atoms together with the appearance of the flat dispersion connecting the two valley K and K' points [Fig. 2(a1)]. The gap of the bulk is closed. The armchair edge is characterized by the absence of exponentially localized edge channels together with the absence of zero-energy edge states [Fig. 2(b1)].

It is intriguing to investigate how these properties are modified by the SOI.[22] According to the bulk-edge correspondence, once the SOI is introduced, the edge channels of graphene without the SOI turn into the topologically protected ones. On one hand, in the case of zigzag edges, the flat zero-energy edge modes begin to cant and yield the helical modes intrinsic to the QSH insulator [Figs. 2(a2) and 2(a3)]. Zero-energy states remain even if the width W of the nanoribbon is quite narrow. On the other hand, in the case of armchair edges, the absence of the zero-energy edge modes must continue despite the bulk-edge correspondence even if the SOI is introduced because the band structure cannot be modified discontinuously by any adiabatic process [Figs. 2(b2) and 2(b3)]. As we demonstrate, what actually occurs reads as follows: Zero-energy states emerge but disappear from the energy spectrum due to an interference of two edge states. As a result, we predict the emergence of the density of states (DOS) along the edge as remnants of zero-energy edge states. The observation of the DOS may be used as experimental evidence that silicene is a topological insulator.

The penetration depth ($\xi_{\rm zig}$,$\xi_{\rm arm}$) of the helical edge channel plays the key role in understanding the mechanism by which the difference arises between the zigzag and armchair nanoribbons from the viewpoint of the topological protection and the hybridization between the two edges.[23,24] We derive a geometrical relation $\xi_{\rm zig}\xi_{\rm arm} = \frac{\sqrt{3}}{2}a^2$, with a the lattice constant. The SOI and the topology play completely different roles between the armchair and zigzag nanoribbons, though the topologically protected helical edge channels appear in both cases.

The basic nature of silicene is described by the model[7]

$$H = -t\sum_{\langle i,j\rangle\alpha} c^\dagger_{i\alpha}c_{j\alpha} + i\frac{\lambda_{\rm SO}}{3\sqrt{3}}\sum_{\langle\langle i,j\rangle\rangle\alpha\beta}\nu_{ij}c^\dagger_{i\alpha}\sigma^z_{\alpha\beta}c_{j\beta}, \qquad (1)$$

where $c^\dagger_{i\alpha}$ creates an electron with spin polarization α at site i in a honeycomb lattice, and $\langle i,j\rangle/\langle\langle i,j\rangle\rangle$ run over all the nearest/next-nearest-neighbor hopping sites. The first term represents the usual nearest-neighbor hopping with the transfer energy $t = 1.6$ eV, while the second term represents the effective SOI[6,25] with $\lambda_{\rm SO} = 3.9$ meV, where $\boldsymbol{\sigma} = (\sigma_x,\sigma_y,\sigma_z)$ is the Pauli matrix of spin, with $\nu_{ij} = +1$ if the next-nearest-neighboring hopping is anticlockwise and $\nu_{ij} = -1$ if it is clockwise with respect to the positive z axis.

Silicene has a buckled structure separating the sublattice planes for A sites and B sites by a distance $2\ell = 0.46$ Å. It generates a staggered sublattice potential $\propto 2\ell E_z$ between

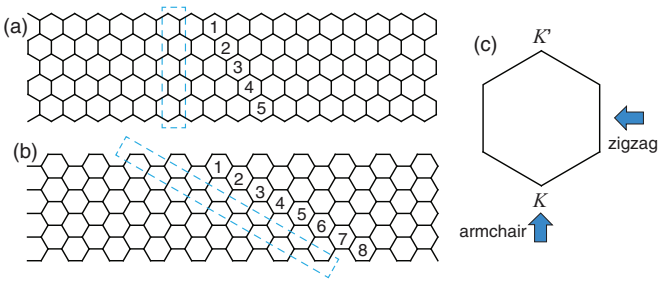

FIG. 1. (Color online) Illustration of (a) zigzag and (b) armchair nanoribbons. Its width W is defined by the number of hexagons in a unit cell. Here we have taken $W = 5$ for zigzag and $W = 8$ for armchair nanoribbons. (c) The hexagonal Brillouin zone. The states near the Fermi energy are π orbitals residing near the K and K' points at opposite corners of the hexagonal Brillouin zone. The bulk band structure of nanoribbons is obtained by projecting the band structure of the bulk from the direction depicted in the figure. The K and K' points are identified in the armchair edge.

silicon atoms at A sites and B sites in electric field E_z.[10] Furthermore, we may generate the Haldane interaction[26] term with strength λ_Ω by way of photoirradiation.[11] It is also possible to include the staggered exchange magnetization[12] with strength ΔM. They are summarized as an additional term ΔH to the Hamiltonian (1),

$$\Delta H = -\ell \sum_{i\alpha} \mu_i E_z c_{i\alpha}^\dagger c_{i\alpha} + i\frac{\lambda_\Omega}{3\sqrt{3}} \sum_{\langle\langle i,j\rangle\rangle\alpha\beta} \nu_{ij} c_{i\alpha}^\dagger c_{j\beta} + \Delta M \sum_{i\alpha} \mu_i c_{i\alpha}^\dagger \sigma_z c_{i\alpha}, \quad (2)$$

where $\mu_i = \pm 1$ for i representing the A (B) site. This additional term provides silicene with enormously rich physics.

We define the width W of the nanoribbon as the number of hexagons in a unit cell as shown in Fig. 1. The unit cell contains $2W + 4$ ($2W + 2$) silicon atoms for armchair (zigzag) nanoribbons. We have diagonalized numerically the Hamiltonian (1) to obtain the eigenvalues and the eigenstates, from which we find the band structure and the wave function.

We start with a gedanken experiment by changing the parameter λ_{SO} in the Hamiltonian (1). In Fig. 2, we show the evolution of the dispersions of the electronic states as the SOI is increased for zigzag [(a1)–(a3)] and armchair [(b1)–(b3)] nanoribbons, respectively. There are two types of gaps: one for the edge part (2δ) and the other for the bulk part (2Δ). In the case of zigzag nanoribbons, the flat dispersion begins to cant and yield the helical modes intrinsic to the QSH insulator as the SOI is introduced [Figs. 2(a2) and 2(a3)]. Furthermore, the gap 2δ of the edge channel remains zero while the gap 2Δ of the bulk states becomes finite and increases as the SOI is increased. On the other hand, in the case of armchair nanoribbons, the gap 2δ due to the finite size effect decreases, while the gap 2Δ increases as the SOI is increased [Figs. 2(b1)–2(b3)].

We show the width dependence of the gap 2δ for several fixed values of λ_{SO} in Fig. 3. The gap oscillates in the period of three, as is a well-known feature[20] of armchair nanoribbons. When $\lambda_{SO} = 0$ ($\lambda_{SO} \neq 0$), the gap decreases antipropotionally (exponentially) as W increases for $\mathrm{mod}_3 W \neq 0$. The gap approached zero for wider armchair nanoribbons.

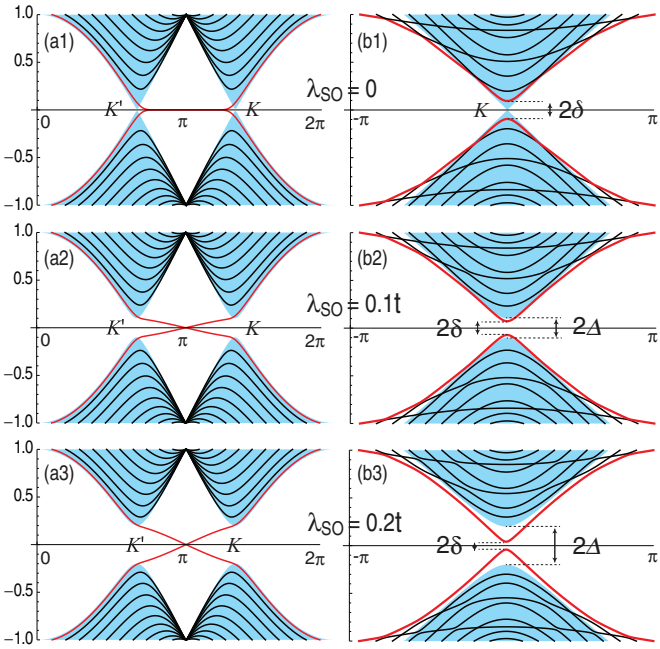

FIG. 2. (Color online) Band structure of [(a1)–(a3)] zigzag and [(b1)–(b3)] armchair nanoribbons. We have taken $\lambda_{SO} = 0$ for (a1) and (b1), $\lambda_{SO}/t = 0.1$ for (a2) and (b2), and $\lambda_{SO}/t = 0.2$ for (a3) and (b3). We have taken the width $W = 16$. The vertical axis is the energy in a unit of t and the horizontal axis is the momentum k. Zero-energy edge modes are present in the zigzag nanoribbon [(a2) and (a3)] but not in the armchair nanoribbon [(b2) and (b3)], though the bulk is a topological insulator for $\lambda_{SO} \neq 0$ in both cases. The cyan region (red curve) represents the band of the bulk (edge). The bulk spectrum takes the minimum at the K and K' points. (The K and K' points are identified in the armchair nanoribbon.) The bulk mode is well described by the analytic formula (5), while the edge mode is well described by the dispersion relation (11) for an armchair nanoribbon and (13) for a zigzag nanoribbon. The band gap of the bulk (edge) is denoted by 2Δ (2δ), which increases (decreases) as λ_{SO} increases. The horizontal axis is the momentum in a unit of $1/a$, and the vertical axis is the energy in a unit of t.

We show the absolute value of the real-space wave function in Fig. 4. When $\lambda_{SO} = 0$, the wave function is constant for $\mathrm{mod}_3 W = 0$ and almost constant for $\mathrm{mod}_3 W \neq 0$ across the nanoribbon. The peaks emerge at both edges as λ_{SO} increases. They are the zero-energy edge modes required by the bulk-edge correspondence, as we shall soon demonstrate based on analytic formulas. We note that there is a considerable amount of overlap between them. The overlap becomes smaller as λ_{SO} increases. The order of the overlap is measured by the penetration depth ξ of the edge mode.

We proceed to construct the low-energy theory to make a further study of the zero-energy modes and their overlap in a nanoribbon. We adopt the Hamiltonian $H + \Delta H$ in order to apply our results to a realistic material such as silicene. The low-energy theory in the K_η (K or K') valley is given by the Dirac Hamiltonian[10–12,25]

$$H_\eta = \hbar v_F(\eta k_x \tau_x + k_y \tau_y) + \lambda_{SO}\sigma_z \eta \tau_z - \ell E_z \tau_z + \lambda_\Omega \eta \tau_z + \Delta M \sigma_z \tau_z, \quad (3)$$

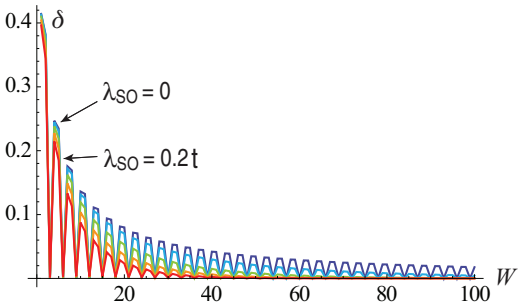

FIG. 3. (Color online) Band gap 2δ of armchair nanoribbons as a function of the width W for various spin-orbit interactions $\lambda_{SO}/t = 0,0.05,0.1,0.15,0.2$ (from top to bottom). The vertical axis is the energy in a unit of t and the horizontal axis is W.

where $v_F = \frac{\sqrt{3}}{2\hbar}at = 5.5 \times 10^5$ m/s is the Fermi velocity with the lattice constant $a = 3.86$ Å, and τ_a the Pauli matrix of the sublattice pseudospin. This Hamiltonian describes a four-component Dirac fermion indexed by the spin $\sigma_z = \pm 1$ and the pseudospin $\tau_z = \pm 1$ for each valley $\eta = \pm 1$.

The coefficient of τ_z is summarized as $\Delta_{s_z}^{\eta}$. It is the mass of the Dirac electron with the spin s_z in the valley η,

$$\Delta_{s_z}^{\eta} = \eta s_z \lambda_{SO} - \ell E_z + \eta \lambda_\Omega + s_z \Delta M. \tag{4}$$

A nontrivial topological charge is generated when $\Delta_{s_z}^{\eta}$ has a different sign in the two valleys. Silicene is a QSH insulator without the external fields ($E_z = 0$, $\lambda_\Omega = 0$, $\Delta M = 0$). The gap is given by $2|\Delta_{s_z}^{\eta}|$. The energy spectrum reads

$$E(k) = \pm\sqrt{(\hbar v_F)^2 k^2 + \left(\Delta_{s_z}^{\eta}\right)^2}, \tag{5}$$

which is illustrated by taking $\Delta_{s_z}^{\eta} = \lambda_{SO}$ in Fig. 2. It gives a good approximation to the band structure of the bulk.

We investigate the zero-energy edge modes of armchair nanoribbons. We take the x direction as the translational direction of a nanoribbon. The zero-energy edge modes appear at $k_x = 0$. The transverse momentum k_y is determined by solving $E(k_y) = 0$ with (5), or $k_y = \pm i|\Delta_{s_z}^{\eta}|/(\hbar v_F)$. The wave function for the edge located at $\pm L$ reads

$$\psi_{\pm L}(y) = \Theta(|y| - L) \exp\left[\pm \frac{|\Delta_{s_z}^{\eta}|}{\hbar v_F}(y \mp L)\right], \tag{6}$$

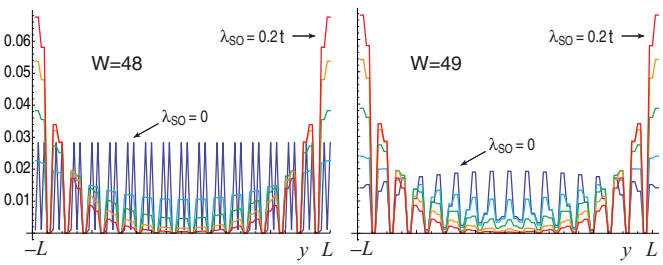

FIG. 4. (Color online) Real-space wave function of armchair nanoribbons near the Fermi energy for SOI $\lambda_{SO}/t = 0,0.05,0.1,0.15,0.2$. We take (a) $W = 48$ and (b) $W = 49$. Note that $\mathrm{mod}_3 48 = 0$ and $\mathrm{mod}_3 49 = 1$. The horizontal axis is the y axis of the nanoribbon with the width $2L$.

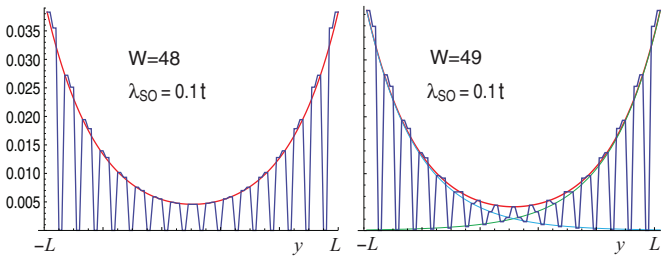

FIG. 5. (Color online) Real-space wave function of armchair nanoribbons near the Fermi energy. The bonding state (8) obtained analytically presents a good fit of the numerically determined wave function. Here we take examples of $W = 48$ and 49. The horizontal axis is the y axis of the nanoribbon with the width $2L$.

up to a normalization constant, where $\Theta(|y| - L) = 1$ for $|y| < L$ and $\Theta(|y| - L) = 0$ for $|y| > L$. Here, L and W are related as $L = \frac{1}{2}Wa$. The penetration depth is given by

$$\xi_{\mathrm{arm}} = \hbar v_F / \left|\Delta_{s_z}^{\eta}\right|. \tag{7}$$

We have demonstrated the emergence of the zero-energy modes (6) at the two edges ($y = \pm L$). They are the ones required by the bulk-edge correspondence.

However, their wave functions mix due to the interedge interaction, and form the bonding state given by

$$\psi_+(y) = [\psi_{+L}(y) + \psi_{-L}(y)]/\sqrt{2} = \cosh(y/\xi_{\mathrm{arm}}), \tag{8}$$

up to a normalization constant. The wave functions (6) and (8) present remarkably good approximations to the envelope functions of the numerically calculated wave functions (Fig. 5).

The energy of the bonding state is estimated as $-S$, with

$$\begin{aligned} S &= \frac{\left|\Delta_{s_z}^{\eta}\right|}{2L}\int_{-L}^{L} \psi_{-L}^*(y)\psi_{+L}(y)dy \\ &= \left|\Delta_{s_z}^{\eta}\right| \exp\left(-2L/\xi_{\mathrm{arm}}\right). \end{aligned} \tag{9}$$

The ground state is no longer the zero-energy state but the bonding states with a negative energy. This is why the zero-energy edge modes disappear from the energy spectrum of armchair nanoribbons.

The effective Hamiltonian of the armchair edge states reads

$$H = \sigma_z \tau_z^{\mathrm{edge}} \hbar v_F k_x + S\tau_x^{\mathrm{edge}}, \tag{10}$$

where τ_i^{edge} is the Pauli matrix for the edge pseudospin and $\tau_z^{\mathrm{edge}} = \pm 1$ for the top and bottom edges. The first term describes the two edge states ($\tau_z^{\mathrm{edge}} = \pm 1$) with the opposite velocity each of which carries the up and down spins ($\sigma_z = \pm 1$). The second term describes the mixing of the two edge states. By diagonalizing the Hamiltonian (10), the eigenvalue is

$$E = \pm\sqrt{(\hbar v_F)^2 k_x^2 + S^2}. \tag{11}$$

This gives a good approximation of the edge mode in Fig. 2, where $S \approx \delta$. The overlap integral produces the gap of the edge states.

Finally, we investigate zigzag nanoribbons with the SOI. We show the absolute value of the real-space wave function in Fig. 6. The edge state in one edge is completely localized at A sites, while the other edge is completely localized at B sites

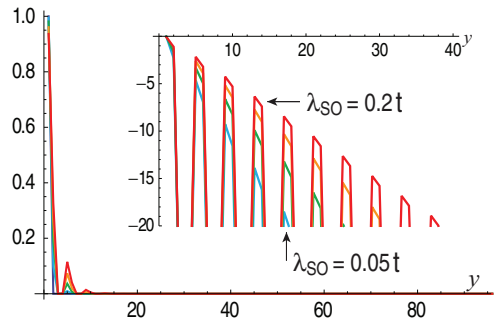

FIG. 6. (Color online) Real-space wave function of zigzag nanoribbons at the Fermi energy for SOI $\lambda_{SO}/t = 0, 0.05, 0.1, 0.15, 0.2$. They are well described by the analytic formula (14). Inset: A logarithm plot of the wave functions. Clearly it decreases linearly as the position increases. We take $W = 24$.

when $\lambda_{SO} = 0$. The two states localized at the two edges are orthogonal to each other, and there is exactly no overlap between the two edge modes. Furthermore, the penetration depth is zero. When $\lambda_{SO} \neq 0$, although the totally localized state is not an exact solution, the wave function is almost localized at the edge. The overlap between the two edge states is found to be zero within the accuracy of our numerical calculation.

The edge mode crosses the Fermi energy $k_x = \pi$ as in Figs. 2(a2) and 2(a3). Since the Dirac Hamiltonian (3) describes solely the low-energy theory near the K and K' points separately, it does not provide us with the low-energy Hamiltonian of a zigzag nanoribbon connecting the tips of the two Dirac cones. Nevertheless we are able to write down the phenomenological Hamiltonian for the zigzag edge states,

$$H = \sigma_z \tau_z^{\text{edge}} \lambda_{SO} \hbar v_F k_x / t, \tag{12}$$

by requiring a linear dispersion,

$$E = \pm \lambda_{SO} \hbar v_F k_x / t, \tag{13}$$

as is the result of numerical analysis. The electron velocity in the edge states is almost constant and proportional to the SOI λ_{SO}. This dispersion gives an excellent fitting of the zero-energy edge mode as in Figs. 2(a2) and 2(a3).

The wave function of the zero-energy state is well fitted by

$$\psi_{\pm L}(y) = \Theta(|y| - L) \exp[\pm(y \mp L)/\xi_{\text{zig}}], \tag{14}$$

where the penetration depth is approximately given by

$$\xi_{\text{zig}} \simeq a \left| \Delta_{s_z}^{\eta} \right| / t. \tag{15}$$

It is interesting that the penetration depths of zigzag and armchair edges have a universal relation,

$$\xi_{\text{arm}} \xi_{\text{zig}} \simeq a \hbar v_F / t = \frac{\sqrt{3}}{2} a^2, \tag{16}$$

where the right-hand side is the area of a hexagon. The geometrical meaning of this relation is yet to be explored.

We have shown that zero-energy modes emerge both in zigzag and armchair nanoribbons as required by the bulk-edge correspondence. Although they disappear from the energy spectrum in armchair nanoribbons because of an interference of the two edge states, their remnant is experimentally detectable by scanning tunneling microscopy. This makes the crucial difference from graphene nanoribbon with armchair edges, and would present the simplest experimental evidence that silicene is a topological insulator.

In passing we make some comments. First, the gap 2δ of the armchair nanoribbon is of the order of 10 meV when the width is 10 μm. The gap 2δ in the edge channel is observable in armchair nanoribbons. This offers an interesting possibility to construct the ideal situation in which only the Coulomb interaction is effective between the two helical edge channels without the hybridization, where a new electronic liquid state has been proposed.[27] Second, we address the problem of the effect due to edge disorders. The properties of edge states between graphene and silicene nanoribbons are essentially different. The edge channel in silence is topologically protected from the disorder as long as the time-reversal symmetry is preserved and the bulk gap remains finite since silicene is a QSH system, while this is not the case in graphene. Third, we point out that silicene nanoribbons with clean zigzag edges have experimentally been synthesized on the (110) surface of silver crystal.[28] Finally, edge states can also be observed by the transport measurement of silicene nanoribbons.[29]

Note added. Recently, two related papers appeared. One is an experimental observation of DOS peaks due to edge states in silicene.[30] The emergence of edge states in the armchair edge is strong evidence that silicene is a topological insulator. The other paper is a theoretical one, which has some overlap with the present work.[31]

This work was supported in part by Grants-in-Aid for Scientific Research from the Ministry of Education, Science, Sports and Culture No. 22740196 and No. 24224009.

[1] P. Vogt, P. De Padova, C. Quaresima, J. Avila, E. Frantzeskakis, M. C. Asensio, A. Resta, B. Ealet, and G. Le Lay, Phys. Rev. Lett. **108**, 155501 (2012).

[2] C.-L. Lin, R. Arafune, K. Kawahara, N. Tsukahara, E. Minamitani, Y. Kim, N. Takagi, and M. Kawai, Appl. Phys. Express **5**, 045802 (2012).

[3] A. Fleurence, R. Friedlein, T. Ozaki, H. Kawai, Y. Wang, and Y. Yamada-Takamura, Phys. Rev. Lett. **108**, 245501 (2012).

[4] L. Chen, C. C. Liu, B. Feng, X. He, P. Cheng, Z. Ding, S. Meng, Y. Yao, and K. Wu, Phys. Rev. Lett. **109**, 056804 (2012).

[5] B. Feng, Z. Ding, S. Meng, Y. Yao, X. He, P. Cheng, L. Chen, and K. Wu, Nano Lett. **12**, 3507 (2012).

[6] C.-C. Liu, W. Feng, and Y. Yao, Phys. Rev. Lett. **107**, 076802 (2011).

[7] C. L. Kane and E. J. Mele, Phys. Rev. Lett. **95**, 226801 (2005); **95**, 146802 (2005)

[8] H. Min, J. E. Hill, N. A. Sinitsyn, B. R. Sahu, L. Kleinman, and A. H. MacDonald, Phys. Rev. B **74**, 165310 (2006).

[9] Y. Yao, F. Ye, X.-L. Qi, S.-C. Zhang, and Z. Fang, Phys. Rev. B **75**, 041401 (2007).

[10]M. Ezawa, New J. Phys. **14**, 033003 (2012).
[11]M. Ezawa, Phys. Rev. Lett. **110**, 026603 (2013).
[12]M. Ezawa, Phys. Rev. B **87**, 155415 (2013).
[13]M. Ezawa, Phys. Rev. Lett. **109**, 055502 (2012).
[14]M. Z. Hasan and C. Kane, Rev. Mod. Phys. **82**, 3045 (2010).
[15]X.-L. Qi and S.-C. Zhang, Rev. Mod. Phys. **83**, 1057 (2011).
[16]C. Wu, B. A. Bernevig, and S.-C. Zhang, Phys. Rev. Lett. **96**, 106401 (2006).
[17]C. Xu and J. E. Moore, Phys. Rev. B **73**, 045322 (2006).
[18]B. A. Bernevig, T. L. Hughes, and S. C. Zhang, Science **314**, 1757 (2006).
[19]M. Fujita, K. Wakabayashi, K. Nakada, and K. Kusakabe, J. Phys. Soc. Jpn. **65**, 1920 (1996).
[20]M. Ezawa, Phys. Rev. B **73**, 045432 (2006).
[21]L. Brey and H. A. Fertig, Phys. Rev. B **73**, 235411 (2006).
[22]J. W. Rhim and K. Moon, Phys. Rev. B **84**, 035402 (2011).
[23]B. Zhou, H.-Z. Lu, R.-L. Chu, S.-Q. Shen, and Q. Niu, Phys. Rev. Lett. **101**, 246807 (2008).
[24]H.-Z. Lu, W.-Y. Shan, W. Yao, Q. Niu, and S. Q. Shen, Phys. Rev. B **81**, 115407 (2010).
[25]C.-C. Liu, H. Jiang, and Y. Yao, Phys. Rev. B **84**, 195430 (2011).
[26]F. D. M. Haldane, Phys. Rev. Lett. **61**, 2015 (1988).
[27]Y. Tanaka and N. Nagaosa, Phys. Rev. Lett. **103**, 166403 (2009).
[28]B. Aufray, A. Kara, S. Vizzini, H. Oughaddou, C. Leandri, B. Ealet, and G. L. Lay, Appl. Phys. Lett. **96**, 183102 (2010); P. D. Padova, C. Quaresima, C. Ottaviani, P. M. Sheverdyaeva, P. Moras, C. Carbone, D. Topwal, B. Olivieri, A. Kara, H. Oughaddou, B. Aufray, and G. L. Lay, *ibid*. **96**, 261905 (2010).
[29]M. Ezawa, Appl. Phys. Lett. **102**, 172103 (2013).
[30]B. Feng, H. Li, C.-C. Liu, T. Shao, P. Cheng, Y. Yao, S. Meng, L. Chen, and K. Wu, arXiv:1304.3308.
[31]L. Cano-Cortes, C. Ortix, and J. van den Brink, arXiv:1303.2252.